

Electrically-programmable frequency comb for compact quantum photonic circuits

Shakir Ullah,¹ Mehmet Emre Tasgin,¹ Rasim Volga Ovali,² and Mehmet Günay³

¹*Institute of Nuclear Sciences, Hacettepe University, 06800 Ankara, Turkey*

²*Department of Physics, Recep Tayyip Erdogan University, 53100 Rize, Turkey*

³*Department of Nanoscience and Nanotechnology, Faculty of Arts and Science, Burdur Mehmet Akif Ersoy University, 15030 Burdur, Turkey*

(Dated: August 2, 2023)

Recent efforts have demonstrated the first prototypes of compact and programmable photonic quantum computers (PQCs). Utilization of time-bin encoding in loop-like architectures enabled programmable generation of quantum states and execution of different (programmable) logic gates on a single circuit. Actually, there is still space for better compactness and complexity of available quantum states: photonic circuits (PCs) can function at different frequencies. This necessitates an optical component which can make different frequencies talk with each other. This component should be integrable into PCs and be controlled –preferably– by voltage for programmable generation of multifrequency quantum states and PQCs. Here, we propose such a device which controls four-wave mixing process, essential for frequency combs. We utilize nonlinear Fano resonances. Entanglement generated by the device can be tuned continuously by the applied voltage which can be delivered to the device via nm-thick wires. The device is integrable, CMOS-compatible, and operates within a timescale of hundreds of femtoseconds.

I. INTRODUCTION

Demonstrations of quantum supremacy over classical computers [1, 2] intensified the research on integrated quantum circuits (IQCs) where generation, processing, and detection of quantum states can be carried out on a single chip [3, 4]. This increased the demand for scalable integration of nonlinear optical components, such as squeezers [5, 6], frequency combs [7] and other nonlinearity generators, into IQC chips. Though integration of various nonlinear components into IQCs are demonstrated successfully [8], nonlinearity (for squeezing and entanglement) generation in such devices are either fixed [9] or cannot be tuned conveniently [10–13].

In order to achieve the quantum supremacy on a wider range of computations, it is necessary to build programmable quantum computers (QCs) [14–20], in which flexible quantum states can be generated [14, 18] and various logic gates can be implemented [16–18]. In state-of-the-art PQCs, a given initial squeezing (nonclassicality) is supplied to the circuit on the first module and different entangled states are produced via variable beam-splitters (VBSs) and phase-shifters [14, 18]. In the current PQCs, information is encoded in a pulse train where each pulse corresponds to a mode within the time-domain multiplexing [21]. The pulses (modes) are made interact with each other in a loop-structure in order to obtain several-dimensional entangled states. That is, tunability of, for instance, squeezing is rather a new concept [22]. Computation can also be performed in similar loop-like architectures where different logic gates can be implemented using measurement-induced squeezing protocol with VBSs [16–18]. A single circuit can execute a universal gate [23] by winding the input pulse in that programmable circuit.

Such a loop architecture provides extreme compactness regarding both quantum state preparation and comput-

ing. Nevertheless, there is more to do with the compactness and complexity of PQCs [24]. A given circuit can function at different frequencies [7]. If one can entangle (link) the pulses of different frequencies [25], the functionality of the PQCs can be increased tremendously. For this reason, a close attention is paid on scalable (integrated) frequency combs [7, 24–26]. While important achievements are obtained, the fabricated combs are not conveniently (electrically) programmable, yet.

A frequency comb employs, e.g., four-wave mixing (FWM) process, where central (pump) pulse is split into two side bands. The new side bands also yield other side bands, resulting a comb of different frequencies. Thus, if one can control the FWM process, she/he can program the frequency comb.

Here, we propose a device where the FWM process can be controlled (continuously tuned) by an applied voltage [11, 27–29] which can be delivered through nm-thick wires. The device is integrable into quantum photonic circuits and CMOS-compatible. A quantum emitter (QE), located at the hot-spot of a plasmonic nanostructure (PNS), introduces a Fano resonance in the nonlinear response [30, 31], see Figs. 1 and 3. Depending on the QE’s resonance Ω_{QE} , the FWM process ($\omega_3 = 1.8\omega_1$) can either be turned off (at $\Omega_{QE} = \omega_3 = 1.8000\omega_1$) or can be further enhanced (at $\Omega_{QE} \simeq 1.8005\omega_1$) on top of the field-enhanced FWM of the bare nanostructure, see Fig. 3. (Here, ω_1 is the pump frequency used in scaling and $\omega_3 = 1.8\omega_1$ corresponds to the FWM frequency.)

Fano resonances take place at sharp frequency intervals [32, 33]. This may be disadvantageous for broadband enhancement of nonlinearity. However, here it becomes extremely useful for programming the FWM process via a meV-tuning of the QE’s resonance [11, 27, 28]. One should also note that while plasmonic excitations decay in a few femtoseconds, quantum optics experiments with plasmons [34–39] clearly show that they can handle quan-

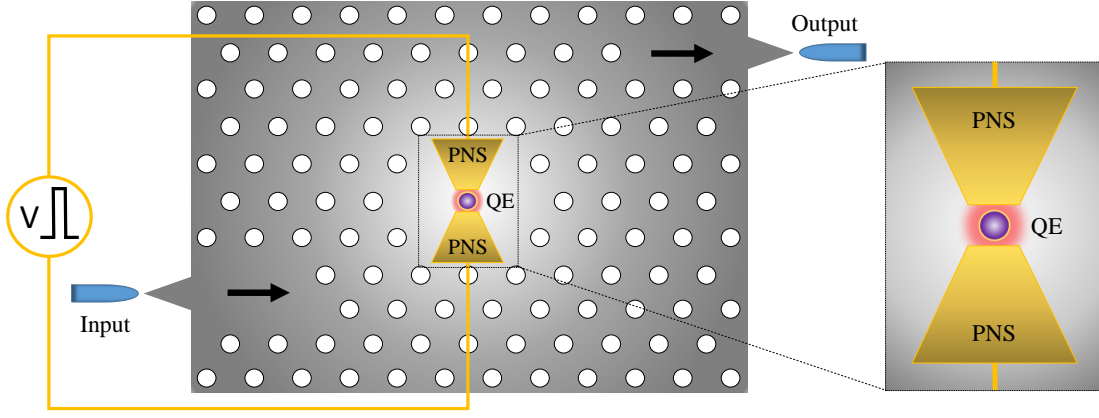


FIG. 1. Control mechanism of programmable frequency comb which introduces configurable links (entanglement) among different frequency modes in an IQC. A PNS is placed in a photonic cavity. The resonance of the QE, positioned at the hotspot of the PNS, is controlled electrically via a voltage applied over the PNS itself. The QE resonance controls the FWM process (see Fig. 3) taking place within the device. Cyclic use of the FWM process generates a frequency comb [7]. Thus, the links among different frequency components can be programmed electrically.

tum features, like squeezing and entanglement, as long as 0.1 nanoseconds. The latter is determined by noise features [40].

In the proposed device, the QE resonance is electrically-tuned by an applied voltage, which is delivered to the QE over the nanostructure itself. A few volts is more than sufficient for the tuning $\Omega_{QE} = 1.8000 - 1.8005 \times \omega_1$. This corresponds to a continuous-control over the FWM intensity, where modulation depths as high as 5 orders of magnitude can be achieved, see Fig. 3. That is, entanglement among the different frequency modes can be continuously-tuned (programmed, linked) in the same manner, see Fig. 4. Similarly, the single-mode nonclassicalities (e.g., squeezing) of the modes can be continuously-tuned, see Fig. 1 in the Supplementary Material (SM) [41].

Therefore, the proposed device provides an electrically-programmable frequency comb for quantum computers and information processing. The programming ability (tunability) of the device is continuous. The device provides a tremendous compactness and extremely enhanced complexity for the information processing due to the existence of programmable links between different frequency modes. The links among frequencies can be implemented using the off-line measurement-induced protocols [42] rather than directly coupling the fragile quantum states to nonlinear media.

Below, we first describe the dynamics of the FWM process taking place in the proposed device where a PNS-QE coupled system is placed into a photonic cavity. (QE can be a quantum dot, defect-center in a 2D material or nanoparticle whose resonance can be electrically tuned.) We obtain Langevin equations governing the dynamics of plasmon and cavity modes given in Fig. 2. Before calculating the entanglement among different frequencies, we demonstrate the enhancement of the FWM intensity

using c-numbers (semiclassical) at their steady-states, see Fig. 3. Next, we calculate the entanglement (Fig. 4) and squeezing using the noise operators [43–46].

Dynamics of the coupled system.— The scheme of the device, dynamics of the FWM process and entanglement generation can be described as follows. The PNS, e.g., a bow-tie antenna depicted in Fig. 1, is placed into a photonic cavity which supports the three related modes (\hat{c}_{1-3} , resonances $\Omega_{c1}-\Omega_{c3}$) for the FWM process, see Fig. 2. The \hat{c}_1 and \hat{c}_2 cavity modes are pumped with two integrated lasers of frequencies ω_1 and ω_2 , hamiltonian $\hat{\mathcal{H}}_{\text{las-cav}}$. The cavity fields interact (strengths g_{1-3}) with the plasmon modes (\hat{a}_{1-3}) of the PNS, see resonances $\Omega_{a1}-\Omega_{a3}$ in Fig. 2 respectively; hamiltonian $\hat{\mathcal{H}}_{\text{cav-pls}}$. PNS localizes the cavity fields into hot-spots which appears at the centre, e.g., for the bow-tie structure. Localization not only enhances the hot-spot field intensities by orders of magnitude, but also increases the overlap integrals for the nonlinear processes [30, 31, 47], here for the FWM. Because of the notorious increase in the overlap integral, nonlinear conversion takes place over plasmons [48]. The FWM frequency is $\omega_3 = 2\omega_1 - \omega_2$. That is, two plasmons in \hat{a}_1 is annihilated and one plasmon in \hat{a}_2 and one plasmon in \hat{a}_3 modes are generated, hamiltonian $\hat{\mathcal{H}}_{\text{FWM}}$.

The QE is positioned at the hot-spot of the PNS. QE's resonance, Ω_{QE} , is chosen such that its coupling (strength f) takes place mainly with the FWM plasmon mode (Ω_{a3}), hamiltonian $\hat{\mathcal{H}}_{\text{pls-QE}}$. (Choice of the values for Ω_{QE} in Figs. 3 and 4 justifies this notion.)

Including also energies of the QE, plasmon and cavity modes, hamiltonian $\hat{\mathcal{H}}_0$, the total hamiltonian can be written as

$$\hat{\mathcal{H}} = \hat{\mathcal{H}}_0 + \hat{\mathcal{H}}_{\text{las-cav}} + \hat{\mathcal{H}}_{\text{cav-pls}} + \hat{\mathcal{H}}_{\text{FWM}} + \hat{\mathcal{H}}_{\text{pls-QE}}, \quad (1)$$

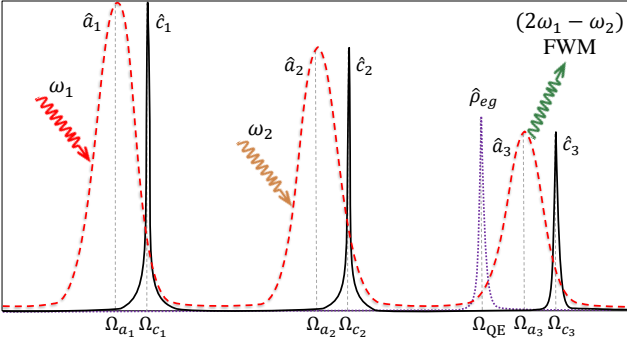


FIG. 2. Resonances of the cavity ($\hat{c}_{1,2,3}$, $\Omega_{c1,2,3}$) and plasmon ($\hat{a}_{1,2,3}$, $\Omega_{a1,2,3}$) modes. Resonance of the QE Ω_{QE} is selected around the Ω_{a3} plasmon mode into which FWM oscillations $\omega_3 = 2\omega_1 - \omega_2$ take place.

where

$$\hat{\mathcal{H}}_0 = \hbar\Omega_{QE} \hat{\rho}_{ee} + \hbar \sum_{i=1}^3 (\Omega_{a_i} \hat{a}_i^\dagger \hat{a}_i + \Omega_{c_i} \hat{c}_i^\dagger \hat{c}_i), \quad (2)$$

$$\hat{\mathcal{H}}_{\text{las-cav}} = i\hbar(\hat{c}_1^\dagger \varepsilon_L^{(1)} e^{-i\omega_1 t} + \hat{c}_2^\dagger \varepsilon_L^{(2)} e^{-i\omega_2 t} - \text{H.c.}), \quad (3)$$

$$\hat{\mathcal{H}}_{\text{cav-pls}} = \hbar(g_1 \hat{c}_1 \hat{a}_1^\dagger + g_2 \hat{c}_2 \hat{a}_2^\dagger + g_3 \hat{c}_3 \hat{a}_3^\dagger + \text{H.c.}), \quad (4)$$

$$\hat{\mathcal{H}}_{\text{FWM}} = \hbar\chi_{\text{FWM}}(\hat{a}_3^\dagger \hat{a}_2^\dagger \hat{a}_1^2 + \hat{a}_1^\dagger \hat{a}_2 \hat{a}_3), \quad (5)$$

$$\hat{\mathcal{H}}_{\text{pls-QE}} = \hbar(f\hat{a}_3^\dagger \hat{\rho}_{ge} + f\hat{a}_3 \hat{\rho}_{eg}). \quad (6)$$

Here, $\hat{\rho}_{ee} = |e\rangle\langle e|$, $\hat{\rho}_{eg} = |e\rangle\langle g|$ and $\hat{\rho}_{ge} = \hat{\rho}_{eg}^\dagger$ represent the density matrices for the QE [46]. $\varepsilon_L^{(1)}$ and $\varepsilon_L^{(2)}$ are the pump amplitudes/strengths. χ_{FWM} is the overlap integral [30, 31, 47] for the plasmon modes involving in the FWM process.

Entanglement is originally created among the plasmon modes in the first place. The plasmon modes interact with the cavity modes via a beam-splitter interactions ($\hat{c}_i^\dagger \hat{a}_i + \text{H.c.}$). This transfers the squeezing [49] into the cavity modes. Moreover, cavity modes are entangled with each other due to entanglement swap mechanism [50]. That is, the entanglement among plasmon modes is swapped into the entanglement among the cavity modes. Cavity modes interact with the cavity output modes $\hat{c}_{\text{out}}^{(1-3)}$ in a similar manner. Thus, the produced multimode entanglement finally swaps into the entanglement among the cavity output modes of three different frequencies.

We mention more about the calculation method of the entanglement in the following paragraphs, but the basics of the mechanism responsible for the entanglement generation is given in the above paragraph. By controlling the QE resonance with an applied voltage, one can control the FWM and the degree of entanglement (link) between different frequencies.

Time-evolution of the modes and QE can be obtained from the Heisenberg equations of motion, e.g., $i\hbar\dot{\hat{a}} = [\hat{a}, \hat{H}]$. Including also the damping/decay rates for the

cavity fields ($\kappa_{1-3} = 10^5$ Hz), plasmon fields ($\gamma_{1-3} = 10^{14}$ Hz) and the QE ($\gamma_{eg} = 10^9$ Hz), the Langevin equations can be written as

$$\dot{\hat{c}}_1 = -(\kappa_1 + i\Omega_{c1})\hat{c}_1 - ig_1^* \hat{a}_1 + \varepsilon_L^{(1)} e^{-i\omega_1 t}, \quad (7)$$

$$\dot{\hat{c}}_2 = -(\kappa_2 + i\Omega_{c2})\hat{c}_2 - ig_2^* \hat{a}_2 + \varepsilon_L^{(2)} e^{-i\omega_2 t}, \quad (8)$$

$$\dot{\hat{c}}_3 = -(\kappa_3 + i\Omega_{c3})\hat{c}_3 - ig_3^* \hat{a}_3, \quad (9)$$

$$\dot{\hat{a}}_1 = -(\gamma_1 + i\Omega_{a1})\hat{a}_1 - ig_1 \hat{c}_1 - i2\chi_{\text{FWM}} \hat{a}_1^\dagger \hat{a}_2 \hat{a}_3, \quad (10)$$

$$\dot{\hat{a}}_2 = -(\gamma_2 + i\Omega_{a2})\hat{a}_2 - ig_2 \hat{c}_2 - i\chi_{\text{FWM}} \hat{a}_3^\dagger \hat{a}_1^2, \quad (11)$$

$$\dot{\hat{a}}_3 = -(\gamma_3 + i\Omega_{a3})\hat{a}_3 - ig_3 \hat{c}_3 - if\rho_{ge} - i\chi_{\text{FWM}} \hat{a}_2^\dagger \hat{a}_1^2, \quad (12)$$

$$\dot{\hat{\rho}}_{ge} = -(\gamma_{eg} + i\Omega_{QE})\hat{\rho}_{ge} + if\hat{a}_3(\hat{\rho}_{gg} - \hat{\rho}_{ee}), \quad (13)$$

$$\dot{\hat{\rho}}_{ee} = -\gamma_{ee}\hat{\rho}_{ee} + if\hat{a}_3^\dagger \hat{\rho}_{ge} - if\hat{a}_3 \hat{\rho}_{eg}. \quad (14)$$

Here, γ_{ee} and γ_{eg} are the diagonal and off-diagonal elements decay rates of the QE.

Fano-control of the FWM process.— We calculate the entanglement/squeezing by investigating the noise features (e.g., $\delta\hat{c}$) of the operators around their steady-state values (c-numbers) $\alpha_c = \langle\hat{c}\rangle$ with $\hat{c} = \alpha + \delta\hat{c}$. Thus, we first calculate the expectations α for the modes and investigate the fluctuations $\delta\hat{c}$ about them. The calculation of the expectations reveals also the Fano-control (suppression and enhancement) mechanism as follows.

We replace the operators in the Langevin equations (7)-(14) with their expectations. We determine their steady-state values α_{c1-c3} and α_{a1-a3} , see Sec. 2 of SM [41]. For instance, $|\alpha_{a3}|^2$ gives the number of generated FWM plasmons at the frequency ω_3 . As described in Sec. 2 of the SM [41], an analytical expression for the FWM plasmon amplitude can be obtained as

$$\alpha_{a3} = \frac{i\chi_{\text{FWM}}\alpha_{a2}^* \alpha_{a1}^2}{\frac{|f|^2 y}{i(\Omega_{QE} - \omega_3) + \gamma_{eg}} - (i(\Omega_{a3} - \omega_3) + \gamma_3)}, \quad (15)$$

with $y = \rho_{ee} - \rho_{gg}$ and $\omega_3 = 2\omega_1 - \omega_2$. While we also calculate the numerical values for α_{a3} in Fig. 3, this expression depicts the essential idea below the nonlinearity control. An interference taking place in the denominator of Eq. (15) is in charge for the enhancement of the FWM.

The resonance of the QE Ω_{QE} can be arranged (tuned) so that the imaginary part of the first term in the denominator cancels the expression $i(\Omega_{a3} - \omega_3)$ in the second term. This gives the peak in Fig. 3. We note that enhancement factor (EF) given in Fig. 3 multiplies the EFs originating due to the field localization enhancements [30].

On the contrary, FWM process can be turned off for the choice of $\Omega_{QE} = \omega_3$. In this case, the FWM frequency ω_3 production is suppressed. This can be observed from Eq. (15) as follows. $\Omega_{QE} = \omega_3$, the first term of the denominator becomes $|f|^2 y / \gamma_{eg}$ which turns out to be extremely large because of the small decay rate, e.g., $\gamma_{eg} = 10^{-6}\omega_1$, of the QE [11]. We scale frequencies by ω_1 . The second term of the denominator is below unity

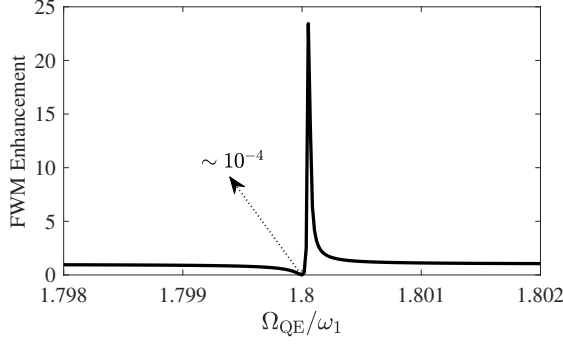


FIG. 3. Control of FWM process via the choice of the QE resonance. Plotted enhancement factor (EF) multiplies the EF due to local field enhancement [51]. FWM process can be tuned continuously between 10^{-4} ($\Omega_{QE} = \omega_3 = 1.8000\omega_1$) and 25 ($\Omega_{QE} = \omega_3 = 1.8005\omega_1$) via voltage applied on the QE [11, 27–29].

and can be neglected besides $|f|^2 y / \gamma_{eg}$. Thus, the FWM intensity $|\alpha_{a_3}|^2$ is suppressed by orders of magnitude, see the dip (10^{-4}) in Fig. 3.

Control of entanglement and squeezing.— The links among different frequency modes can also be controlled by the applied voltage. Entanglement and squeezing features are determined by the quantum fluctuations (quantum noise $\delta\hat{c}_i$) about the expectation values $\alpha_{c_i} = \langle\hat{c}_i\rangle$ [45]. We employ a standard method [43, 44] in our calculations. Equations of motions for the noise operators are obtained by inserting, e.g., the expressions $\hat{c}_i = \alpha_i + \delta\hat{c}_i$, into the Langevin equations (7)–(14), and including the noise operators $\delta\hat{c}_{in}^{(i)}(t) = -i \sum_k e^{-i\omega_k^{(i)}t} \hat{b}_k^{(i)}(0)$, see Sec. 3 of the SM [41]. (\hat{b}_k are vacuum modes, so $\hat{c}_{in}^{(i)}$ is the vacuum noise [45].) Ignoring the higher order terms in the equations for the noise operators [43, 44], one obtains

$$\delta\dot{\hat{c}}_1 = -(\kappa_1 + i\Delta_{c_1})\delta\hat{c}_1 - ig_1^* \delta\hat{a}_1 + \delta\hat{c}_{in}^{(1)}(t), \quad (16)$$

$$\delta\dot{\hat{c}}_2 = -(\kappa_2 + i\Delta_{c_2})\delta\hat{c}_2 - ig_2^* \delta\hat{a}_2 + \delta\hat{c}_{in}^{(2)}(t), \quad (17)$$

$$\delta\dot{\hat{c}}_3 = -(\kappa_3 + i\Delta_{c_3})\delta\hat{c}_3 - ig_3^* \delta\hat{a}_3, \quad (18)$$

$$\delta\dot{\hat{a}}_1 = -(\Gamma_1 + i\Delta_{a_1})\delta\hat{a}_1 - ig_1 \delta\hat{c}_1 - i2\chi_{FWM} \times (\alpha_{a_1}^* \alpha_{a_2} \delta\hat{a}_3 + \alpha_{a_1}^* \delta\hat{a}_2 \alpha_{a_3} + \delta\hat{a}_1^\dagger \alpha_{a_2} \alpha_{a_3}), \quad (19)$$

$$\delta\dot{\hat{a}}_2 = -(\Gamma_2 + i\Delta_{a_2})\delta\hat{a}_2 - ig_2 \delta\hat{c}_2 - i\chi_{FWM} \times (2\alpha_{a_3}^* \alpha_{a_1} \delta\hat{a}_1 + \delta\hat{a}_3^\dagger \alpha_{a_1}^2), \quad (20)$$

$$\delta\dot{\hat{a}}_3 = -(\Gamma_3 + i\Delta_{a_3})\delta\hat{a}_3 - ig_3 \delta\hat{c}_3 - i\chi_{FWM} \times (2\alpha_{a_2}^* \alpha_{a_1} \delta\hat{a}_1 + \delta\hat{a}_2^\dagger \alpha_{a_1}^2). \quad (21)$$

where $\Delta_{c_i} = \omega_{c_i} - \omega_i$ and $\Delta_{a_i} = \omega_{a_i} - \omega_i$, with $i = 1, 2, 3$, represent detuning of the cavity and plasmonic modes from the laser fields.

We note that the damping rates Γ_{1-3} we use for the plasmonic noise operators $\delta\hat{a}_{1-3}$ are different than the

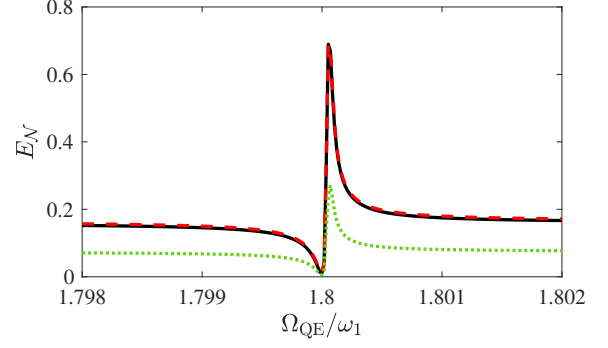


FIG. 4. Entanglement in units of log-neg (E_N) [52–55] between different frequency output modes of the cavity: $\hat{c}_{out}^{(1)} - \hat{c}_{out}^{(2)}$ (solid black line), $\hat{c}_{out}^{(1)} - \hat{c}_{out}^{(3)}$ (red dashed line) and $\hat{c}_{out}^{(2)} - \hat{c}_{out}^{(3)}$ (dotted green line). Entanglement can be continuously tuned by applied voltage which is below a single volt.

ones γ_{1-3} we use in calculating the decay of plasmon excitations. This is due to the following fact. The experiments with PNSs clearly demonstrate [34–39] that plasmon excitations can handle nonclassicality features (entanglement and squeezing), determined by the noise operators [40], for times as long as 10^{-10} s. This is only one order lower than, e.g., a quantum dot. We use $\Gamma_{1-3} = 10^{10}$ Hz in our calculation.

We calculate the entanglement among the three output modes of the cavity $\hat{c}_{out}^{(1-3)}$ each operating at different frequencies ω_{1-3} . The output modes are obtained from $\hat{c}_{out}^{(i)} = r_i \hat{c}_i(t) + \hat{c}_{in}^{(i)}$ using the input-output formalism [45, 46], where r_i are constants related with the cavity-vacuum coupling rates. See Sec. 3 of the SM [41].

We use logarithmic negativity (log-neg, E_N) for quantifying the entanglement [52–56]. Log-neg is a measure [55] of entanglement for Gaussian states. The linearization treatment [43, 44], we employ here, leaves the quantum states Gaussian, so that here we can use log-neg as a measure. We also measure the nonclassicality (e.g., squeezing) of the output modes in units of log-neg. We employ the concept of entanglement-potential [57], which weighs the nonclassicality of a mode in terms of the entanglement it generates after a beams-splitter [57, 58].

In Fig. 4, we present the log-neg entanglement among the three output frequency modes of the cavity, i.e., $\hat{c}_{out}^{(1)} - \hat{c}_{out}^{(2)}$, $\hat{c}_{out}^{(2)} - \hat{c}_{out}^{(3)}$, and $\hat{c}_{out}^{(1)} - \hat{c}_{out}^{(3)}$. Tuning the QE resonance between $\Omega_{QE} = 1.8000\omega_1$ and $1.8005\omega_1$, one can continuously control the entanglement (link) between different frequencies. The interval $1.8005 - 1.8000 = 0.0005\omega_1$ corresponds to sub-meV tuning for a typical QE. For instance, in the experiment [27] 1 Volt can tune a QD about 10 meV and much better ones are available [11, 28, 29, 59, 60].

Summary and outlook.— Recent efforts seek programmable and compact QCs capable of generating and executing configurable quantum states and logic gates. An IQC can function at different frequencies. The recent

compactness provided by the employment of time-bin encoding [16–18, 21] can be tremendously enhanced by enabling different frequency modes of the IQC to interact with each other [7, 24–26]. Here, we demonstrate the generation of programmable links among different frequency modes, leading to ultra-compact programmable QCs where links can be configured among time-bin encoded photons (modes) functioning at different frequencies. Programmed links among different frequency operations can be established via measurement-induced protocol [42] without directly coupling the fragile quantum states into nonlinear media. The device operates at sub-

picosecond frequencies and is CMOS-compatible. Thus, the device provides a game-changing increase in the capacity, compactness, and controllability of QCs.

ACKNOWLEDGMENTS

SU, MET and RVO acknowledge support from TÜBİTAK-1001 Grant No. 121F141. MET and MG is funded by TÜBİTAK-1001 Grant No. 117F118.

-
- [1] A. W. Harrow and A. Montanaro, Quantum computational supremacy, *Nature* **549**, 203 (2017).
 - [2] H.-S. Zhong, H. Wang, Y.-H. Deng, M.-C. Chen, L.-C. Peng, *et al.*, Quantum computational advantage using photons, *Science* **370**, 1460 (2020).
 - [3] G. Masada, K. Miyata, A. Politi, T. Hashimoto, J. L. O’Brien, and A. Furusawa, Continuous-variable entanglement on a chip, *Nat. Photonics* **9**, 316 (2015).
 - [4] V. D. Vaidya, B. Morrison, L. G. Helt, R. Shahrokshahi, D. H. Mahler, *et al.*, Broadband quadrature-squeezed vacuum and nonclassical photon number correlations from a nanophotonic device, *Sci. Adv.* **6**, eaba9186 (2020).
 - [5] F. Mondain, T. Lunghi, A. Zavatta, E. Gouzien, F. Doutre, *et al.*, Chip-based squeezing at a telecom wavelength, *Photon. Res.* **7**, A36 (2019).
 - [6] Y. Zhang, M. Menotti, K. Tan, V. Vaidya, D. Mahler, *et al.*, Squeezed light from a nanophotonic molecule, *Nat. Commun.* **12**, 2233 (2021).
 - [7] M. Kues, C. Reimer, J. M. Lukens, W. J. Munro, A. M. Weiner, D. J. Moss, and R. Morandotti, Quantum optical microcombs, *Nat. Photonics* **13**, 170 (2019).
 - [8] E. Pelucchi, G. Fagas, I. Aharonovich, D. Englund, E. Figueroa, *et al.*, The potential and global outlook of integrated photonics for quantum technologies, *Nat. Rev. Phys.* **4**, 194 (2022).
 - [9] Y. Zhao, Y. Okawachi, J. K. Jang, X. Ji, M. Lipson, and A. L. Gaeta, Near-degenerate quadrature-squeezed vacuum generation on a silicon-nitride chip, *Phys. Rev. Lett.* **124**, 193601 (2020).
 - [10] X. Lu, G. Moille, A. Rao, D. A. Westly, and K. Srinivasan, Efficient photoinduced second-harmonic generation in silicon nitride photonics, *Nat. Photonics* **15**, 131 (2021).
 - [11] D. Hallett, A. P. Foster, D. L. Hurst, B. Royall, P. Kok, *et al.*, Electrical control of nonlinear quantum optics in a nano-photonic waveguide, *Optica* **5**, 644 (2018).
 - [12] A. P. Foster, D. Hallett, I. V. Iorsh, S. J. Sheldon, M. R. Godsand, *et al.*, Tunable photon statistics exploiting the fano effect in a waveguide, *Phys. Rev. Lett.* **122**, 173603 (2019).
 - [13] M. Wang, N. Yao, R. Wu, Z. Fang, S. Lv, J. Zhang, J. Lin, W. Fang, and Y. Cheng, Strong nonlinear optics in on-chip coupled lithium niobate microdisk photonic molecules, *New J. Phys.* **22**, 073030 (2020).
 - [14] L. S. Madsen, F. Laudenbach, M. F. Askarani, F. Rortais, T. Vincent, *et al.*, Quantum computational advantage with a programmable photonic processor, *Nature* **606**, 75 (2022).
 - [15] W. Asavanant, B. Charoensombutamon, S. Yokoyama, T. Ebihara, T. Nakamura, *et al.*, Time-domain-multiplexed measurement-based quantum operations with 25-mhz clock frequency, *Phys. Rev. Appl.* **16**, 034005 (2021).
 - [16] M. V. Larsen, X. Guo, C. R. Breum, J. S. Neergaard-Nielsen, and U. L. Andersen, Deterministic multi-mode gates on a scalable photonic quantum computing platform, *Nat. Phys.* **17**, 1018 (2021).
 - [17] S. Takeda and A. Furusawa, Universal quantum computing with measurement-induced continuous-variable gate sequence in a loop-based architecture, *Phys. Rev. Lett.* **119**, 120504 (2017).
 - [18] J. M. Arrazola, V. Bergholm, K. Brádler, T. R. Bromley, M. J. Collins, *et al.*, Quantum circuits with many photons on a programmable nanophotonic chip, *Nature* **591**, 54 (2021).
 - [19] Y. Enomoto, K. Yonezu, Y. Mitsuhashi, K. Takase, and S. Takeda, Programmable and sequential gaussian gates in a loop-based single-mode photonic quantum processor, *Sci. Adv.* **7**, eabj6624 (2021).
 - [20] F. Arute, K. Arya, R. Babbush, D. Bacon, J. C. Bardin, R. Barends, *et al.*, Quantum supremacy using a programmable superconducting processor, *Nature* **574**, 505 (2019).
 - [21] S. Yokoyama, R. Ukai, S. C. Armstrong, C. Sornphiphatphong, T. Kaji, *et al.*, Ultra-large-scale continuous-variable cluster states multiplexed in the time domain, *Nat. Photonics* **7**, 982 (2013).
 - [22] M. Günay, P. Das, E. Yüce, E. O. Polat, A. Bek, and M. E. Tasgin, On-demand continuous-variable quantum entanglement source for integrated circuits, *Nanophotonics* **12**, 229 (2023).
 - [23] S. L. Braunstein and P. van Loock, Quantum information with continuous variables, *Rev. Mod. Phys.* **77**, 513 (2005).
 - [24] L. Caspani, C. Reimer, M. Kues, P. Roztock, M. Clerici, *et al.*, Multifrequency sources of quantum correlated photon pairs on-chip: a path toward integrated quantum frequency combs, *Nanophotonics* **5**, 351 (2016).
 - [25] H. Mahmudlu, R. Johanning, A. Van Rees, A. Khodadad Kashi, J. P. Epping, *et al.*, Fully on-chip photonic turnkey quantum source for entangled qubit/qudit state

- generation, *Nat. Photonics* **17**, 518 (2023).
- [26] M. Kues, C. Reimer, P. Roztock, L. R. Cortés, S. Sciara, *et al.*, On-chip generation of high-dimensional entangled quantum states and their coherent control, *Nature* **546**, 622 (2017).
- [27] K. Shibata, H. Yuan, Y. Iwasa, and K. Hirakawa, Large modulation of zero-dimensional electronic states in quantum dots by electric-double-layer gating, *Nature Commun.* **4**, 1 (2013).
- [28] C. Chakraborty, L. Kinnischtzke, K. M. Goodfellow, R. Beams, and A. N. Vamivakas, Voltage-controlled quantum light from an atomically thin semiconductor, *Nat. Nanotechnol.* **10**, 507 (2015).
- [29] S. Schwarz, A. Kozikov, F. Withers, J. K. Maguire, A. P. Foster, *et al.*, Electrically pumped single-defect light emitters in wse₂, *2D Mater.* **3**, 025038 (2016).
- [30] S. K. Singh, M. K. Abak, and M. E. Tasgin, Enhancement of four-wave mixing via interference of multiple plasmonic conversion paths, *Phys. Rev. B* **93**, 035410 (2016).
- [31] M. E. Tasgin, A. Bek, and S. Postacı, Fano resonances in the linear and nonlinear plasmonic response, *Fano Resonances in Optics and Microwaves: Physics and Applications* **219** (2018).
- [32] S. Postacı, B. C. Yildiz, A. Bek, and M. E. Tasgin, Silent enhancement of sers signal without increasing hot spot intensities, *Nanophotonics* **7**, 1687 (2018).
- [33] M. Günay, V. Karanikolas, R. Sahin, R. V. Ovali, A. Bek, and M. E. Tasgin, Quantum emitter interacting with graphene coating in the strong-coupling regime, *Phys. Rev. B* **101**, 165412 (2020).
- [34] S. Fasel, F. Robin, E. Moreno, D. Erni, N. Gisin, and H. Zbinden, Energy-time entanglement preservation in plasmon-assisted light transmission, *Phys. Rev. Lett.* **94**, 110501 (2005).
- [35] M. S. Tame, K. McEnery, Ş. Özdemir, J. Lee, S. A. Maier, and M. Kim, Quantum plasmonics, *Nat. Phys.* **9**, 329 (2013).
- [36] S. Fasel, M. Halder, N. Gisin, and H. Zbinden, Quantum superposition and entanglement of mesoscopic plasmons, *New J. Phys.* **8**, 13 (2006).
- [37] A. Huck, S. Smolka, P. Lodahl, A. S. Sørensen, A. Boltasheva, J. Janousek, and U. L. Andersen, Demonstration of quadrature-squeezed surface plasmons in a gold waveguide, *Phys. Rev. Lett.* **102**, 246802 (2009).
- [38] S. Varró, N. Kroó, D. Oszetzky, A. Nagy, and A. Czitrovsky, Hanbury brown–twiss type correlations with surface plasmon light, *J. Mod. Opt.* **58**, 2049 (2011).
- [39] G. Di Martino, Y. Sonnefraud, S. Kéna-Cohen, M. Tame, S. K. Özdemir, M. Kim, and S. A. Maier, Quantum statistics of surface plasmon polaritons in metallic stripe waveguides, *Nano Lett.* **12**, 2504 (2012).
- [40] R. Simon, N. Mukunda, and B. Dutta, Quantum-noise matrix for multimode systems: U(n) invariance, squeezing, and normal forms, *Phys. Rev. A* **49**, 1567 (1994).
- [41] See Supplemental Material.
- [42] R. Filip, P. Marek, and U. L. Andersen, Measurement-induced continuous-variable quantum interactions, *Phys. Rev. A* **71**, 042308 (2005).
- [43] C. Genes, A. Mari, P. Tombesi, and D. Vitali, Robust entanglement of a micromechanical resonator with output optical fields, *Phys. Rev. A* **78**, 032316 (2008).
- [44] D. Vitali, S. Gigan, A. Ferreira, H. Böhm, P. Tombesi, A. Guerreiro, V. Vedral, A. Zeilinger, and M. Aspelmeyer, Optomechanical entanglement between a movable mirror and a cavity field, *Phys. Rev. Lett.* **98**, 030405 (2007).
- [45] C. Gardiner, P. Zoller, and P. Zoller, *Quantum noise: a handbook of Markovian and non-Markovian quantum stochastic methods with applications to quantum optics* (Springer Science & Business Media, 2004).
- [46] M. O. Scully and M. S. Zubairy, *Quantum Optics* (Cambridge University Press, New York, 1997).
- [47] P. Ginzburg, A. Krasavin, Y. Sonnefraud, A. Murphy, R. J. Pollard, S. A. Maier, and A. V. Zayats, Nonlinearly coupled localized plasmon resonances: Resonant second-harmonic generation, *Phys. Rev. B* **86**, 085422 (2012).
- [48] N. B. Grosse, J. Heckmann, and U. Woggon, Nonlinear plasmon-photon interaction resolved by k-space spectroscopy, *Phys. Rev. Lett.* **108**, 136802 (2012).
- [49] W. Ge, M. E. Tasgin, and M. S. Zubairy, Conservation relation of nonclassicality and entanglement for gaussian states in a beam splitter, *Phys. Rev. A* **92**, 052328 (2015).
- [50] A. Sen, U. Sen, Č. Brukner, V. Bužek, M. Żukowski, *et al.*, Entanglement swapping of noisy states: A kind of superadditivity in nonclassicality, *Phys. Rev. A* **72**, 042310 (2005).
- [51] J. Renger, R. Quidant, N. Van Hulst, S. Palomba, and L. Novotny, Free-space excitation of propagating surface plasmon polaritons by nonlinear four-wave mixing, *Phys. Rev. Lett.* **103**, 266802 (2009).
- [52] K. Życzkowski, P. Horodecki, A. Sanpera, and M. Lewenstein, Volume of the set of separable states, *Phys. Rev. A* **58**, 883 (1998).
- [53] G. Vidal and R. F. Werner, Computable measure of entanglement, *Phys. Rev. A* **65**, 032314 (2002).
- [54] G. Adesso, A. Serafini, and F. Illuminati, Extremal entanglement and mixedness in continuous variable systems, *Phys. Rev. A* **70**, 022318 (2004).
- [55] M. B. Plenio, Logarithmic negativity: A full entanglement monotone that is not convex, *Phys. Rev. Lett.* **95**, 090503 (2005).
- [56] S. Tserkis and T. C. Ralph, Quantifying entanglement in two-mode gaussian states, *Phys. Rev. A* **96**, 062338 (2017).
- [57] J. K. Asbóth, J. Calsamiglia, and H. Ritsch, Computable measure of nonclassicality for light, *Phys. Rev. Lett.* **94**, 173602 (2005).
- [58] M. E. Tasgin, Measuring nonclassicality of single-mode systems, *J. Phys. B: At. Mol. Opt. Phys.* **53**, 175501 (2020).
- [59] J. Müller, J. Lupton, P. Lagoudakis, F. Schindler, R. Koeppe, A. Rogach, J. Feldmann, D. Talapin, and H. Weller, Wave function engineering in elongated semiconductor nanocrystals with heterogeneous carrier confinement, *Nano Lett.* **5**, 2044 (2005).
- [60] S. A. Empedocles and M. G. Bawendi, Quantum-confined stark effect in single cdse nanocrystallite quantum dots, *Science* **278**, 2114 (1997).